

Phase-Tunable temperature amplifier

F. PAOLUCCI¹, G. MARCHEGIANI^{1,2}, E. STRAMBINI¹ and F. GIAZOTTO¹

¹ *NEST, Istituto Nanoscienze-CNR and Scuola Normale Superiore, I-56127 Pisa, Italy*

² *Dipartimento di Fisica dell'Università di Pisa, Largo Pontecorvo 3, I-56127 Pisa, Italy*

PACS 85.25.Cp – Josephson devices

PACS 74.25.Bt – Thermodynamic properties of superconductors

PACS 85.80.Fi – Thermoelectric devices

Abstract – Coherent caloritronics, the thermal counterpart of coherent electronics, has drawn growing attention since the discovery of heat interference in 2012. Thermal interferometers, diodes, transistors and nano-valves have been theoretically proposed and experimentally demonstrated by exploiting the quantum phase difference between two superconductors coupled through a Josephson junction. So far, the quantum-phase modulator has been realized in the form of a superconducting quantum interference device (SQUID) or a superconducting quantum interference proximity transistor (SQUIPT). Thence, an external magnetic field is necessary in order to manipulate the heat transport. Here, we theoretically propose the first on-chip fully thermal caloritronic device: the phase-tunable temperature amplifier (PTA). Taking advantage of a recently discovered thermoelectric effect in spin-split superconductors coupled to a spin-polarized system, we generate the magnetic flux controlling the transport through a temperature biased SQUIPT by applying a temperature gradient. We simulate the behavior of the device and define a number of figures of merit in full analogy with voltage amplifiers. Notably, our architecture ensures almost infinite input thermal impedance, maximum gain of about 11 and efficiency reaching the 95%. This concept paves the way for applications in radiation sensing, thermal logics and quantum information.

Introduction. – The discovery of thermoionic emission by Fredrick Guthrie in 1873 [1] brought to the invention of the first electronic devices: the diode and triode amplifiers [2]. After more than 100 years, the recent advances of transistor-based technology [3] made possible the design and production of new daily life devices. In the era of energy saving, the common goal in electronics is to increase the device efficiency in order to abate energy losses and pollutant emissions. Anyways, further developments of nowadays technology are bounded by quantum mechanical restrictions to miniaturization and by heat dissipation [4]. The inescapable heat generated in solid-state nano-structures is considered detrimental in electronics. As a consequence, the ability of mastering the heat transport in such structures has been only recently investigated [5], and it could lead to new concepts and capabilities. In this framework, the experimental demonstration in 2012 of heat interference in a SQUID [6] heralded the foundation of the thermal counterpart of coherent electronics: coherent caloritronics [7,8]. Despite it is still distant from the ripeness of electronics, coherent caloritronics is rapidly growing through the design and the realization of ther-

mal analogues of electronic devices, such as heat diodes [6], transistors [9], valves [10], amplifiers [11] and modulators [12]. One of the theoretical foundations of coherent caloritronics resides in the prediction of the periodic dependence of thermal currents across a Josephson junction [13] on the quantum phase difference between the two superconductors [14]. Hence, the resulting thermal modulation acquires a phase-coherent character. So far, quantum interference between Josephson-coupled superconductors has been realized through the use of a SQUID [15] or, more recently, taking advantage from a newly designed SQUIPT [16–18]. Thereby, the thermal transport across caloritronic devices is manipulated by a magnetic flux Φ threading a superconducting ring, and an external source of magnetic field is essential. The last requirement impeded the realization of fully thermal on-chip coherent caloritronic devices up to now. In the last two years, surprisingly large thermoelectric effects in spin-filtered superconducting tunnel junctions have been predicted [21,22] and demonstrated [23]. This discovery enables the direct transduction, for the first time at cryogenic temperatures, of temperature gradients into electrical signals. Here we

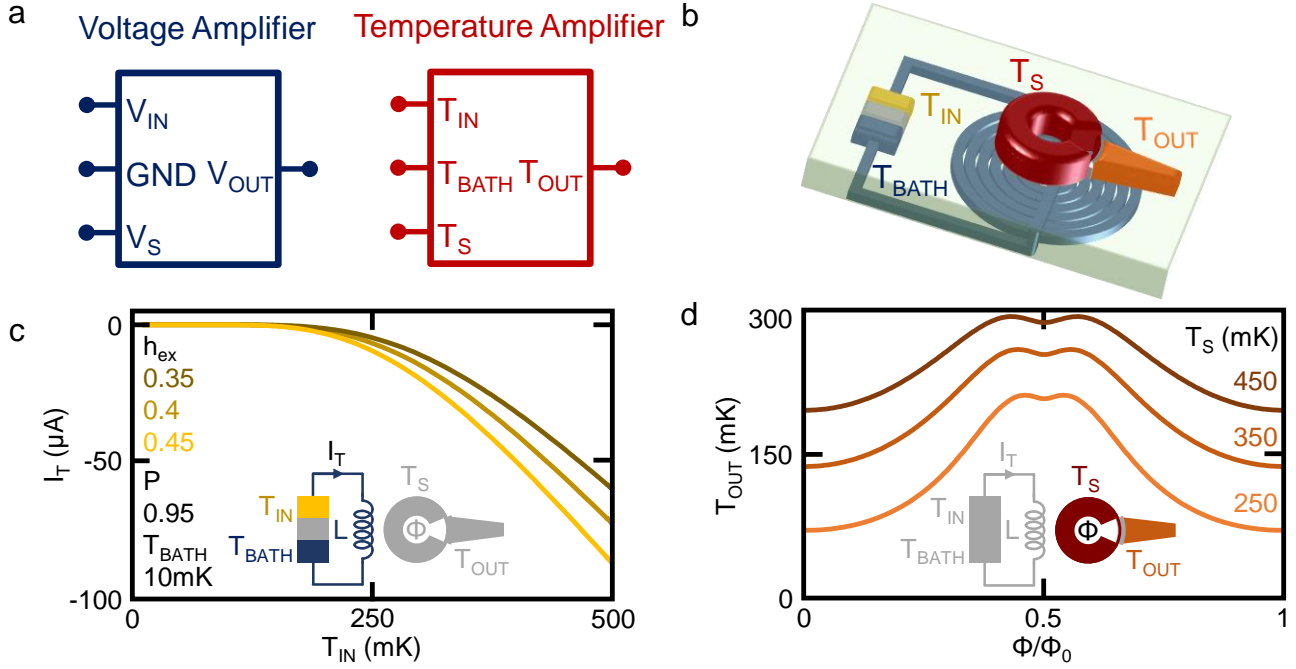


Fig. 1: (a) Circuit diagram symbols of voltage amplifier (blue) and temperature amplifier (red). The input (V_{IN} and T_{IN}), reference (V_{REF} and T_{BATH}) and output (V_{OUT} and T_{OUT}) signals, and the power supplies (V_S and T_S) are represented. (b) Schematic representation of the temperature amplifier: the thermoelectric element highlighted with the dashed rectangle is constituted of a metal (yellow), a ferromagnetic insulator (gray) and a superconductor (turquoise). The turquoise depicts the superconducting coil. The SQUIPT is composed of a S_1N_1 ring (red) and a tunnel-coupled metal probe (orange) through a thin insulator (dark gray). (c) Closed circuit thermoelectric current I_T as a function of T_{IN} for different values of h_{ex} . (d) Output temperature T_{OUT} of the SQUIPT as a function of Φ for different values of T_S . Parameters are listed in the Appendices.

present the first on-chip fully thermal device in caloritronics: the phase-tunable temperature amplifier (PTA). Our architecture takes advantage from the closed-circuit current generated by a thermoelectric element in order to create a magnetic field which controls heat transport across a thermal nano-valve. By employing widely used materials and a geometry feasible with standard lithographic techniques, we show the basic input-to-output temperature conversion, and define several figures of merit in analogy to electronics to evaluate the performances of the temperature amplifier. The device layout may foster its use in different field of science, like quantum information [24], thermal logics [25] and radiation detection [5].

Working principle and basic behavior. – The PTA is the caloritronic equivalent of the voltage amplifier in electronics [26], since temperature is the thermal counterpart of electric potential. The voltage-temperature analogy is schematized in fig. 1-a, where the usual symbol of voltage amplifiers (blue) and the corresponding representation of temperature amplifiers (red) are depicted. A voltage amplifier is a device which produces an output signal $V_{OUT} = G \Delta V_{IN}$, where $G > 1$ is the gain and $\Delta V_{IN} = V_{IN} - V_{REF}$ is the difference between the input signal V_{IN} and the reference V_{REF} . Since the law of conservation of energy does not allow the creation of energy, the system requires a voltage supply V_S to operate.

Analogously, a temperature amplifier generates an output temperature $T_{OUT} = G T_{IN}$, where T_{IN} is the input signal. In this case, the operation power is supplied by a temperature T_S . Differently from electronics, where the absolute value of the signals has no physical meaning and an arbitrary reference potential is required, in caloritronics the temperature signals can take only positive values and they are always referred to zero temperature (zero energy). Thereby, the base temperature T_{BATH} has a different and more complex role than a simple reference. It defines the background energy level, the operation [10] and the energy losses of the system due to electron-phonon interaction [5]. In the following, we set $T_{BATH} = 10$ mK that ensures low noise and reduced energy losses. The PTA is composed of a normal metal-ferromagnetic insulator-superconductor ($N - FI - S$) tunnel junction inductively coupled to a SQUIPT [16] through a superconducting coil.

In an electronic conductor, a thermoelectric effect can be generated by breaking the electron-hole symmetry in the density of states (DOS) [19]. Recently, it has been shown that this can be efficiently realized in superconductor-based structure: i) by inducing a Zeeman spin-splitting h_{ex} in the quasiparticle DOS, hence breaking the electron-hole symmetry for each spin band, ii) by selecting a specific spin band (spin-filtering) [20, 22]. In our scheme, both the mechanisms are provided by a single ferromagnetic insulator layer of the $N - FI - S$ junction

[27]. A temperature gradient between the normal metal N and the superconductor S generates the thermoelectric signal: an open circuit thermovoltage V_T in the Seebeck regime or a closed circuit thermocurrent I_T in the Peltier regime [27]. In our device, we take advantage of the closed circuit thermocurrent in order to create a magnetic field by means of a superconducting coil of self-inductance L . The superconductor is kept at T_{BATH} while the normal metal is set to the input temperature $T_{IN} > T_{BATH}$, because in this configuration the provided thermocurrent exhibits a monotonic behavior with rising temperature gradient [27]. Figure 1-c shows the dependence of I_T on T_{IN} for different values of h_{ex} . The thermocurrent is a growing function of the spin-splitting of the DOS (i.e. h_{ex}) and abruptly rises when the thermal gradient is greater than a critical value (in our numerical calculation $T_{IN} \geq 200$ mK). The detailed description of the temperature-to-current transduction of the $N - FI - S$ junction is given in the Appendices.

We now turn our attention on the second building block of our device: the thermally biased SQUIPT. It is composed of a normal metal wire N_1 interrupting a superconducting ring S_1 , as portrayed in fig. 1-b. Owing to the good electric contact between N_1 and N_2 , the metal wire acquires a superconducting character through the superconducting proximity effect [28]. A normal metal N_2 probe tunnel-coupled to the wire through a thin insulating layer acts as the output electrode of the device. A magnetic flux Φ threading the ring modulates the density of states of the proximized wire [29, 30] and, as a consequence, the electronic transport between N_1 and N_2 [16, 17]. Analogously, the temperature-biased SQUIPT has been predicted to act as a thermal nano-valve leading to a phase-dependent thermal transport between S_1 and N_1 [10]. The detailed theoretical description of the SQUIPT can be found in the Appendices. The thermal behavior of the nano-valve is resumed in fig. 1-d, where the dependence of T_{OUT} on the magnetic flux Φ for different values of T_S is plotted. The probe temperature is minimum at $\Phi = 0$, where the energy gap is fully induced in the N_1 DOS. When the magnetic field is switched on, the probe temperature increases due to the closure of the minigap [16], reaching a maximum at $\Phi \sim 0.45 \Phi_0$ and slightly lowering for $\Phi \rightarrow \Phi_0/2$ [10]. Furthermore, the maximum value of T_{OUT} increases with T_S while its modulation with Φ softens for large values of the supply temperature. Notably, thermal transport across the SQUIPT is phase-dependent, because it is modulated by the superconducting macroscopic phase difference across the proximized wire [10].

The architecture of the PTA requires to couple these two building blocks. This goal is achieved by means of a superconducting coil of inductance L connected to the thermoelectric element (see fig. 1-b). By placing the thermal nano-valve in the center of this coil is possible to drive the SQUIPT by means of the static magnetic flux generated by the coil. The magnetic flux through the SQUIPT is $\Phi = M I_T$, where M is the mutual inductance between the coil and the SQUIPT. This assembly permits to relate

the input T_{IN} with the output T_{OUT} temperature. As typically done in electronics, it is useful to introduce a parameter which sets the input corresponding to the maximum operating output required (here $T_{OUT_{MAX}}$). This quantity is typically called sensitivity (here we use the symbol $Sens$). As already seen (fig 1-d), the temperature of the output probe N_2 increases monotonically with the flux for values smaller than $\sim 0.45\Phi_0$, where it reaches a maximum. Furthermore, the thermocurrent, hence the flux, increases monotonically with the input temperature. If we define $I_{T_{MAX}}$ as the current generated by the thermoelectric temperature for $T_{IN} = Sens$, the coupling required is $M = 0.45\Phi_0/I_{T_{MAX}}$ and the output is a growing function of the input signal, as normally required to an amplifier. Note that the coupling inductance scales inversely with the sensitivity (i.e. $Sens \sim 1/M$). This is not surprising: if we consider a high operating temperature (high $Sens$), a low thermocurrent is sufficient to perform the job.

The basic behavior of the temperature amplifier is illustrated in fig. 2-a, where the dependence of the output temperature T_{OUT} on the input temperature T_{IN} is depicted for a supply temperature $T_S = 250$ mK and for different sensitivities $Sens$. Note that both the minimum and the maximum output temperature are independent on $Sens$. The minimum temperature is obtained at null input signal, i.e. when the normal layer N of the $N - FI - S$ element is at the bath temperature $T_{IN} = T_{BATH}$. For this reason, we refer to it as noise temperature T_{Noise} . The maximum, by definition, is obtained at $T_{IN} = Sens$, corresponding to a flux $0.45\Phi_0$. The horizontal dotted black line sets the minimum value of the output active range $OAR = T_{OUT_{MAX}} - T_{OUT_{MIN}}$ (i.e. the interval where the output varies with the input signal), defined as $T_{OUT_{MIN}} = T_{Noise} + 10\%T_{Noise}$. The size of the OAR is independent on $Sens$ (for our simulation parameters is approximately 130 mK). The independence of the OAR on the $Sens$ may appear surprising at first. However it is easy to understand once it is realized that the OAR is only related on the valve (SQUIPT) operation, whereas $Sens$ only affects the coupling required between the thermoelectric and the valve. On the other hand, T_{OUT} calculated at a specific T_{IN} drops by increasing $Sens$, because the I_T is independent of the sensitivity, and the inducting coupling M lowers by increasing $Sens$.

The supply temperature T_S has a great influence on the behavior of the PTA, because it defines the minimum and the maximum values of T_{OUT} , as illustrated in fig. 2-b. For values of T_S comparable to the critical temperature T_{C-S_1} of the ring of the SQUIPT, T_{OUT} depends only weakly on T_{IN} , because the energy gap of the ring Δ_{S_1} closes and the proximized wire assumes an almost metallic character for every value of the magnetic flux Φ (i.e input temperature T_{IN}). By lowering T_S the superconducting pairing potential rises and the flux Φ successfully modulates thermal transport across the SQUIPT in the complete range $0 - 0.45 \Phi_0$, hence the output temperature varies with all the values of the input signal (see the traces

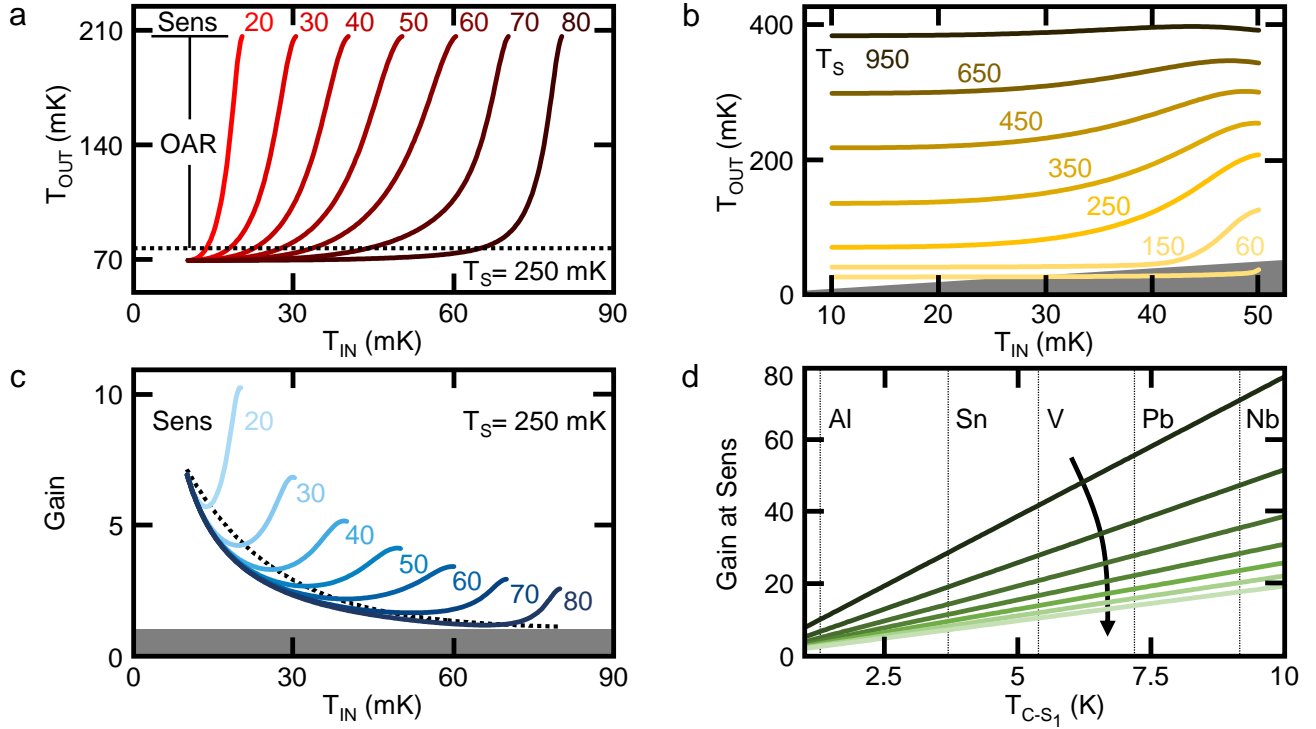


Fig. 2: (a) Output temperature T_{OUT} as a function of T_{IN} calculated for $T_S = 250$ mK and for different values of $Sens$. The black dotted line represents the minimum value of active output $T_{OUT_{MIN}}$. The output active range OAR is shown. (b) Output temperature T_{OUT} as a function of T_{IN} calculated for different values of T_S . The gray triangle depicts the portion of the parameters space with $G \leq 1$. (c) Gain G as a function of T_{IN} calculated for $T_S = 250$ mK and for different values of $Sens$. The gray rectangle represents the area of $G \leq 1$. The black dotted line represents the minimum value of OAR . (d) Gain G as a function of T_{C-S_1} for a constant ratio $T_{C-S_1}/T_S = 5.2$ and different values $Sens$ (increasing with the arrow direction). Cuts at critical temperatures of relevant superconducting materials are represented.

for $T_S = 450 - 150$ mK in fig. 2-b). When $T_S \leq 0.1 T_{C-S_1}$ the thermal broadening of the Fermi distribution $k_B T_S$ is small compared to the energy gap of the ring, and the phase dependence of the thermal transport becomes dominant only when the energy gap is almost fully suppressed, i.e. $\Phi \rightarrow 0.45 \Phi_0$. Thereby, the output temperature is exclusively modulated for $T_{IN} \approx Sens$ and the output signal can be lower than the input, as shown for $T_S = 60$ mK in fig. 2-b. The ensemble of these behaviors leads to the conclusion that the temperature amplifier efficiently works when $0.1 T_{C-S_1} \leq T_S \leq 0.4 T_{C-S_1}$.

The most relevant parameter for an amplifier is the gain G , which is plotted in fig. 2-c as a function of the T_{IN} for different values of $Sens$ and $T_S = 250$ mK. The gain is independent on $Sens$ for $T_{IN} = T_{BATH}$, because T_{Noise} is only determined by T_S . On the contrary, G strongly depends on $Sens$ when the output temperature resides in the OAR (i.e. $T_{OUT} \geq T_{OUT_{MIN}}$). In particular, G lowers by increasing sensitivity at fixed T_{IN} , and $G(T_{IN} = Sens)$ drops for rising $Sens$, because M scales inversely with the sensitivity and the maximum output signal is exclusively controlled by T_S (see fig. 2-a). For a given $Sens$, the gain grows with T_{IN} when the amplifier is in the active output mode, i.e. the values of G above the black dotted line in fig. 2-c. This behavior is the result of the joint

action of the temperature-to-current conversion due to the thermoelectric element and the dependence of the thermal transport across the SQUIPT on the magnetic flux.

Depending on the requirements, one can opt for low values of T_S in order to increase the OAR or choose high values of T_S to maximize G . Since the behavior of the device is satisfactory both in terms of gain and output active range only in a limited range of supply temperatures, the use of materials with higher critical temperature for the ring of the SQUIPT could be beneficial in terms of device performances. Higher values of T_{C-S_1} would guarantee wider OAR and larger G at $T_{IN} = Sens$. The maximum value of the gain in the active region at the optimal constant ratio $T_{C-S_1}/T_S \approx 5.2$ rises linearly with the critical temperature of the SQUIPT for every value of $Sens$, as depicted in fig. 2-d. Therefore, the PTA could potentially be used both at higher values of T_S and T_{IN} ensuring large G and wide OAR too.

Figures of merit. – In full analogy with electronics, we define particular figures of merit for the temperature amplifier. First of all, in our system the input-to-output thermal impedance Z_{IN-OUT}^{th} is infinite. This arises from the double thermal-to-electrical-to-thermal transduction which ensures perfect heat decoupling between the input

load and the output signal. Thereby, no heat current flows directly from the input lead to the output electrode.

Another important parameter is the input amplification range that represents the interval of the input signal for which the output resides in the OAR . The length of this interval IAR is defined as:

$$IAR = Sens - T_{IN}(T_{OUT_{MIN}}), \quad (1)$$

where $T_{IN}(T_{OUT_{MIN}})$ is the value of the input temperature corresponding to the minimum value of the OAR . The IAR is a function both of the T_S and of $Sens$, as illustrated in fig. 3-a. For small values of T_S the OAR is small and, hence, the IAR is not extended too. By rising the supply temperature the IAR enlarges till T_S reaches about 250 mK. A further increase of the supply temperature yields a softening of $\Delta_{S_1}(T)$, and a consequent compression of OAR , as already elucidated above. The reduction of the OAR is mirrored in a narrowing of the IAR . The non-monotonic behavior of the IAR with the $Sens$ comes from the competition between the two terms on the right side of Eq. (1) and can be ascribed to the thermoelectric element. On the one hand, the increase of $Sens$ naturally enlarges the IAR by widening the total input temperature range. On the other hand, I_T rapidly rises with T_{IN} , as illustrated in fig. 1-c. The resulting magnetic flux Φ is modulated only for values of the input temperature approaching $Sens$, because M is small and for the thermocurrents typical of narrow temperature gradients the flux always tends to zero. The latter effect manifests itself in lowering IAR for increasing $Sens$ (see fig. 3-a).

In our amplifier, the temperature is the potential used in the amplification. Hence we can define the efficiency η as:

$$\eta = \frac{T_{OUT_{MAX}}}{T_S} \times 100, \quad (2)$$

where $T_{OUT_{MAX}} = T_{OUT}(T_{IN} = Sens)$. The efficiency reaches $\sim 95\%$ for very small supply temperatures and monotonically decreases with rising T_S , as plotted in fig. 3-b. The drop of η can be explained with the closure of Δ_{S_1} and the growth of the losses through the phonons resulting from the temperature increase [5]. In the region of best performances in terms of OAR , G and IAR (represented with the yellow rectangle in fig. 3-b) the efficiency ranges from $\sim 90\%$ to $\sim 60\%$. These large η values are comparable to analogous commercial electronic amplifiers.

The OAR provides a first and reliable estimate of the useful interval of the output signal. A more complete analysis employs the output dynamic range DR defined as:

$$DR = 20 \times \log \left(\frac{T_{OUT_{MAX}} + T_{Noise}}{T_{Noise}} \right). \quad (3)$$

The DR widens by increasing supply temperature up to $T_S = 150$ mK, because $T_{OUT_{MAX}}$ rises while T_{Noise} is almost unaffected (as shown in the inset of fig. 3-c). Further increase of T_S enlarges the noise with a steeper rate, while $T_{OUT_{MAX}}$ tends to level to a constant value. As a consequence, DR decreases for values of T_S approaching the SQUIPT critical temperature. Despite that, the PTA reaches the maximum performances in terms of DR in the

optimal region in terms of the other figures of merit, as depicted by the turquoise rectangle in fig. 3-c.

Finally, we consider the differential gain, defined as:

$$DG = \frac{dT_{OUT}}{dT_{IN}}. \quad (4)$$

At a fixed sensitivity, DG displays a bell-like shape, as shown in fig. 3-d. The height, width and position of the peak are sensitivity-dependent. In particular, for small and large values of $Sens$ the peak is high and narrow, while for intermediate sensitivities the peak is low and broad in T_{IN} . Since DG is always greater than zero, the output signal is always a monotonically growing function of the input, as required for an amplifier.

Conclusions. – We have proposed the phase-tunable temperature amplifier, which is the caloritronic counterpart of the voltage amplifier in electronics. The pivotal architecture proposed in this work constitutes the first fully-thermal on-chip device in coherent caloritronics, because the magnetic field necessary to control the thermal nano-valve (SQUIPT) is self-generated by the use of a thermoelectric element ($N - FI - S$ junction). The operating principle and the performances have been studied in detail paying specific attention to the experimental feasibility of geometry and material composition. The predicted input-to-output temperature conversion provides a maximum gain $G \approx 11$ at small input signals which is mainly limited by the superconducting critical temperature T_{C-S_1} of the Al-based nano-valve. In addition, we defined several figures of merit in full analogy with voltage amplifiers obtaining remarkable results especially in terms of output dynamic range DR and efficiency η .

The authors acknowledge the European Research Council under the European Unions Seventh Framework Programme (FP7/2007-2013)/ERC Grant No. 615187 - COMANCHE and the MIUR under the FIRB2013 Grant No. RBFR1379UX - Coca for partial financial support. The work of E.S. is funded by a Marie Curie Individual Fellowship (MSCA-IFEF-ST No. 660532-SuperMag).

Appendices. –

N-FI-S junction. The thermoelectric is a tunnel junction made of a normal metal N at temperature T_{IN} , a ferromagnetic insulator FI and a superconductor S at T_{BATH} . The FI layer operates a double action: it behaves as a spin filter with polarization $P = (G_{\uparrow} - G_{\downarrow}) / (G_{\uparrow} + G_{\downarrow})$ where G_{\uparrow} and G_{\downarrow} are the spin up and spin down conductances [32], and it causes the spin-splitting of the DOS of the superconductor by the interaction of its localized magnetic moments with the conducting quasiparticles in S through an exchange field h_{ex} . Since the exchange interaction in a superconductor decays over the coherence length ξ_0 [33], we assume S thinner than ξ_0 and a spatially homogeneous spin-splitting DOS [20]:

$$N_{\uparrow,\downarrow}(E) = \frac{1}{2} \left| \Re \left[\frac{E + i\Gamma \pm h_{ex}}{\sqrt{(E + i\Gamma \pm h_{ex})^2 - \Delta^2}} \right] \right|, \quad (A1)$$

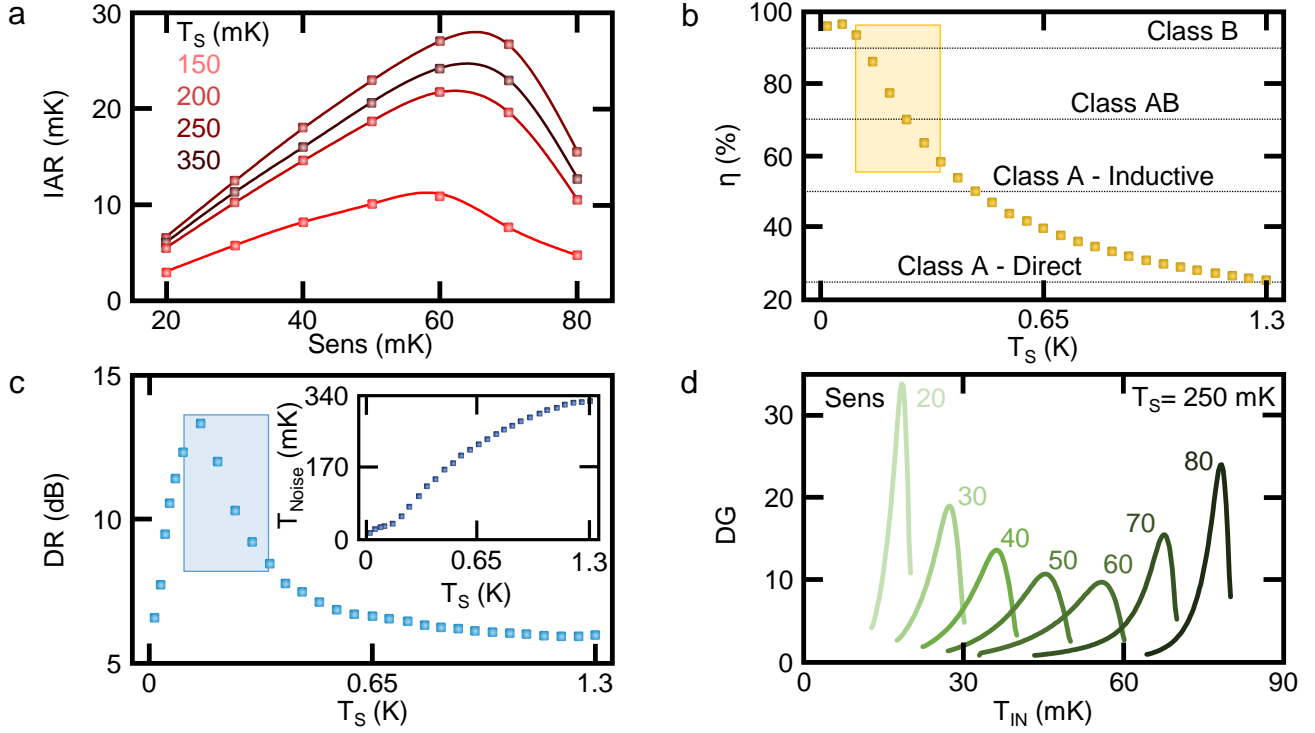


Fig. 3: (a) Amplification range of the input temperature IAR as a function of $Sens$ calculated for different values of T_S . (b) Efficiency η as a function of T_S . The yellow rectangle depicts the area of maximum performances in terms of G and OAR . Typical efficiencies of common voltage amplifiers are shown for a comparison. (c) Output dynamic range DR as a function of T_S . The turquoise rectangle represents the area of maximum performances in terms of G and OAR . Inset: output noise T_{Noise} as a function of T_S . (d) Differential gain DG as a function of T_{IN} calculated at $T_S = 250$ mK for different values of $Sens$.

where E is the energy, Γ is the Dynes parameter accounting for broadening [34], and $\Delta(T_{BATH}, h_{ex})$ is the temperature and exchange field-dependent superconducting energy gap. The pairing potential is calculated self-consistently from the BCS equation [20, 35]:

$$\ln\left(\frac{\Delta_0}{\Delta}\right) = \int_0^{\hbar\omega_D} \frac{f_+(E) + f_-(E)}{\sqrt{E^2 + \Delta^2}} dE \quad (A2)$$

where $f_{\pm}(E) = \left\{1 + \exp\left(\frac{\sqrt{E^2 + \Delta^2} \pm h_{ex}}{k_B T_{BATH}}\right)\right\}^{-1}$ is the Fermi distribution of the electrons, ω_D is the Debye frequency of the superconductor, Δ_0 is the zero-field and zero-temperature superconducting gap, and k_B is the Boltzmann constant. The tunnel thermocurrent in the closed circuit configuration is only due to the temperature gradient and takes the form:

$$I_T = \frac{1}{eR_T} \int_{-\infty}^{\infty} [N_+(E) + PN_-(E)] [f_N(E, T_{IN}) - f_S(E, T_{BATH})] dE, \quad (A3)$$

where e is the electron charge, R_T is the tunnel resistance in the normal state, $N_{\pm}(E) = N_{\uparrow}(E) \pm N_{\downarrow}(E)$, $f_N(E, T_{IN}) = [1 + \exp(E/k_B T_{IN})]^{-1}$ and $f_S(E, T_{BATH}) = [1 + \exp(E/k_B T_{BATH})]^{-1}$ are the metal and superconductor Fermi functions, respectively.

Temperature-biased SQUIPT. We model the SQUIPT as a superconducting ring S_1 interrupted by a one-dimensional normal metal wire N_1 ($l \gg w, t$ where l , w and t are the wire length, width and thickness, respectively). The superconducting properties acquired by the wire through the proximity effect [28] has been shown to

be modulated by the magnetic flux Φ threading the ring [16,17]. Similarly, it has been recently shown that by interrupting the S_1 -loop of the SQUIPT with a superconducting wire S_2 , the superconducting properties of the latter are tuned by the magnetic flux threading the loop [18]. Here we consider a hybrid superconductor-normal metal SQUIPT. Finally, a normal metal N_2 probe is tunnel-coupled to the wire through a thin insulating layer, and acts as output electrode. The DOS of the wire N_{wire} is the real part of the quasi-classical retarded Green's function g^R [36] obtained by solving the one-dimensional Usadel equation [37]. In the short junction limit (i.e. when $E_{Th} = \hbar D/l^2 \gg \Delta_{0S_1}$, where E_{Th} is the Thouless energy, \hbar is the reduced Planck constant and D is the wire diffusion coefficient) the proximity effect is maximized, and the DOS is expressed by [10, 16]:

$$N_{wire}(E, \Phi) = \left| \Re \left[\frac{E - iE_{Th}\gamma g_s}{\sqrt{(E - iE_{Th}\gamma g_s)^2 + [E_{Th}\gamma f_s \cos(\frac{\pi\Phi}{\Phi_0})]^2}} \right] \right|. \quad (A4)$$

Above, $\gamma = R_{N_1}/R_{S_1N_1}$ is the transmissivity of the S_1N_1 contact (with R_{N_1} resistance of the normal wire and $R_{S_1N_1}$ resistance of the S_1N_1 interface), $g_s(E) = \frac{E + i\Gamma_{S_1}}{\sqrt{(E + i\Gamma_{S_1})^2 - \Delta_{S_1}^2}}$ is the coefficient of the phase-independent part of the DOS (with Γ_{S_1} Dynes broadening parameter [34] and Δ_{S_1} BCS temperature dependent energy gap [35]), $f_s(E) = \frac{\Delta_{S_1}}{\sqrt{(E + i\Gamma_{S_1})^2 - \Delta_{S_1}^2}}$ is the

coefficient of the phase-dependent part of the DOS, and $\Phi_0 = 2.068 \times 10^{-15}$ Wb is the magnetic flux quantum. The heat current J tunneling from the S_1N_1 ring to the N_2 probe has been theoretically [5, 10] and experimentally [6, 8, 9] shown to depend on the temperatures of the ring T_S and of the normal electrode T_{OUT} through:

$$J(T_S, T_{OUT}, \Phi) = \frac{2}{e^2 R_{T_1}} \int_0^\infty N_{wire}(E) [f_0(E, T_S) - f_0(E, T_{OUT})] E dE \quad (A5)$$

where $f_0(E, T) = [1 + \exp(E/k_B T)]^{-1}$ is the Fermi distribution of the quasiparticles in the ring for $T = T_S$ and in the probe for $T = T_{OUT}$. The steady-state temperature of the probe T_{OUT} depends on the thermal current flowing from S_1N_1 to N_2 and on the exchange mechanism occurring in N_2 . Below ~ 1 K the relaxation is mainly due to electron-phonon coupling [5] and can be quantified as $J_{e-ph, N_2}(T_{OUT}, T_{BATH}) = \Sigma V (T_{OUT}^n - T_{BATH}^n)$, where Σ is the electron-phonon coupling constant, V is the volume of the probe and the exponent n depends on the disorder of the system. For metals, in the clean limit $n = 5$, while in the dirty limit $n = 4, 6$ [5, 10]. At the steady state by setting a constant temperature of the superconducting ring T_S the output temperature of the nano-valve T_{OUT} can be obtained by solving the following balance equation:

$$-J(T_S, T_{OUT}, \Phi) + J_{e-ph, N_2}(T_{OUT}, T_{BATH}) = 0. \quad (A6)$$

Materials and geometry. The thermoelectric element is composed of 15 nm of Cu as N , 1 nm of EuS as FI and 3 nm of Al as S . Within this geometry the Al layer has typically: $T_C \approx 3$ K, $\Delta_0 \approx 456 \mu\text{eV}$ and $\Gamma = 1 \times 10^{-4} \Delta_0$. We consider an EuS layer characterized by: $P = 0.95$, $h_{ex} = 0.45 \Delta_0$ and $R_T = 0.1 \Omega$. The superconducting coil originating the magnetic flux is made of 10 nm thick aluminum and it is embedded in 10 nm of Al_2O_3 . The SQUIPT is made of a copper N_1 wire ($l = 100$ nm, $w = 30$ nm, $t = 30$ nm) of diffusivity $D = 1 \times 10^{-2} \text{ m}^2/\text{s}$, and of a 150 nm thick Al S_1 ring of radius $r_{SQUIPT} = 5 \mu\text{m}$ with $\Delta_{0-S_1} = 200 \mu\text{eV}$, $T_{C-S_1} \approx 1.32$ K and $\Gamma_{S_1} = 1 \times 10^{-4} \Delta_{0-S_1}$. The transmissivity of the S_1N_1 contact is $\gamma = 33$. The AlMn probe is tunnel-coupled to the proximized wire through a 1 nm thick aluminum oxide layer ($R_{T_1} = 100$ k Ω). The parameters of the AlMn electrode are: $\Sigma = 4 \times 10^9 \text{ WK}^{-6} \text{ m}^{-3}$ [9], $V = 1 \times 10^{-20} \text{ m}^3$ and $n = 6$ [5, 9].

REFERENCES

- [1] GUTHRIE F., *Magnetism and Electricity* (William Collins Sons & Company, Glasgow) 1876.
- [2] GUARNIERI M., *IEEE Ind. Electron. M.*, **6** (2012) 41.
- [3] PUGH E. W., JOHNSON L. R. and PALMER J. H., *IBM's 360 and early 370 Systems* (MIT Press., Cambridge) 1991.
- [4] MANNHART J. and SCHLOM D. G., *Science*, **327** (2010) 1607.
- [5] GIAZOTTO F., HEIKKILÄ T. T., LUUKANEN A., SAVIN A. M. and PEKOLA J. P., *Rev. Mod. Phys.*, **175** (2006) 2171.
- [6] GIAZOTTO F. and MARTINEZ-PÉREZ M. J., *Nature*, **492** (2012) 401.
- [7] MARTINEZ-PÉREZ M. J., SOLINAS P. and GIAZOTTO F., *J Low Temp Phys*, **175** (2014) 813.
- [8] MARTINEZ-PÉREZ M. J., SOLINAS P. and GIAZOTTO F., *Nature Commun.*, **5** (2014) 3579.
- [9] FORNIERI A., BLANC C., BOSISIO R., D'AMBROSIO S. and GIAZOTTO F., *Nat. Nanotech.*, **11** (2015) 258.
- [10] STRAMBINI E., BERGERET F. S. and GIAZOTTO F., *Appl. Phys. Lett.*, **105** (2014) 082601.
- [11] FORNIERI A., TIMOSSO G., BOSISIO R., SOLINAS P. and GIAZOTTO F., *Phys. Rev. B*, **93** (2016) 134508.
- [12] GIAZOTTO F. and MARTINEZ-PÉREZ M. J., *Appl. Phys. Lett.*, **101** (2012) 102601.
- [13] JOSEPHSON B. D., *Phys. Lett.*, **1** (1962) 251.
- [14] MAKI K. and GRIFFIN A., *Phys. Rev. Lett.*, **15** (1965) 921.
- [15] CLARKE J. and BRAGINSKI A. I., eds. *The SQUID Handbook* (Wiley-VCH, Hoboken) 2004.
- [16] GIAZOTTO F., PELTONEN J. T., MESCHKE M. and PEKOLA J. P., *Nat. Phys.*, **6** (2010) 254.
- [17] MESCHKE M., PELTONEN J. T., GIAZOTTO F. and PEKOLA J. P., *Phys. Rev. B*, **84** (2011) 214514.
- [18] VIRTANEN P., RONZANI A. and GIAZOTTO F., *Phys. Rev. Appl.*, **6** (2016) 054002.
- [19] ASHCROFT N. W. and MERMIN D. N., *Solid State Physics* (Saunders College, Belmont) 1976.
- [20] GIAZOTTO F. and TADDEI F., *Phys. Rev. B*, **77** (2008) 132501.
- [21] MACHON P., ESCHRING M. and BELZIG W., *Phys. Rev. Lett.*, **110** (2013) 047002.
- [22] OZAETA A., VIRTANEN P., BERGERET F. S. and HEIKKILÄ T. T., *Phys. Rev. Lett.*, **112** (2016) 057001.
- [23] KOLENDA S., WOLF M. J. and BECKMANN D., *Phys. Rev. Lett.*, **116** (2016) 097001.
- [24] NIELSEN M. A. and CHUANG I. L., *Quantum Computation and Quantum Information* (Cambridge Univ. Press, Cambridge) 2002.
- [25] LI N., REN J., WANG L., ZHANG G., HÄNGGI P. and LI B., *Rev. Mod. Phys.*, **84** (2012) 1045.
- [26] MILLMAN J. and HALKIAS C. C., *Electronic Devices and Circuits* (McGraw-Hill, New York) 1967.
- [27] GIAZOTTO F., SOLINAS P., BRAGGIO A. and BERGERET F. S., *Phys. Rev. Appl.*, **4** (2015) 044016.
- [28] HOLM R. and MEISSNER W., *Z. Phys.*, **74** (1932) 715.
- [29] PETRASHOV V. T., ANTONOV V. N., DELSING P. and CLAESON T., *Phys. Rev. Lett.*, **76** (1995) 5268.
- [30] LE SUEUR H., JOYEZ P., URBINA C. and ESTEVE D., *Phys. Rev. Lett.*, **100** (2008) 197002.
- [31] RONZANI A., ALTIMIRAS C. and GIAZOTTO F., *Phys. Rev. Appl.*, **2** (2014) 024005.
- [32] MOODERA J. S., SANTOS T. S. and NAGAHAMA T., *J. Phys. Condens. Matter*, **19** (2007) 165202.
- [33] TOKUYASU T., SAULS J. A. and RAINER D., *Phys. Rev. B*, **38** (1988) 8823.
- [34] DYNES R. C., GARNO J. P., HERTEL G. B. and ORLANDO T. P., *Phys. Rev. Lett.*, **53** (1984) 2437.
- [35] TINKHAM M., *Introduction to Superconductivity* (McGraw-Hill, New York) 1996.
- [36] RAMMER J. and SMITH H., *Rev. Mod. Phys.*, **58** (1986) 323.
- [37] USADEL K. D., *Phys. Rev. Lett.*, **25** (1970) 507.
- [38] ROSA E. B. and GROVER F. W., *Bulletin of the Bureau of Standards*, **8** (1912) 1.